



HAL
open science

Low-velocity impact of pressurised pipelines

Norman Jones, R.S. Birch

► **To cite this version:**

Norman Jones, R.S. Birch. Low-velocity impact of pressurised pipelines. International Journal of Impact Engineering, 2009, 37 (2), pp.207. 10.1016/j.ijimpeng.2009.05.006 . hal-00641930

HAL Id: hal-00641930

<https://hal.science/hal-00641930>

Submitted on 17 Nov 2011

HAL is a multi-disciplinary open access archive for the deposit and dissemination of scientific research documents, whether they are published or not. The documents may come from teaching and research institutions in France or abroad, or from public or private research centers.

L'archive ouverte pluridisciplinaire **HAL**, est destinée au dépôt et à la diffusion de documents scientifiques de niveau recherche, publiés ou non, émanant des établissements d'enseignement et de recherche français ou étrangers, des laboratoires publics ou privés.

Accepted Manuscript

Title: Low-velocity impact of pressurised pipelines

Authors: Norman Jones, R.S. Birch

PII: S0734-743X(09)00103-1

DOI: [10.1016/j.ijimpeng.2009.05.006](https://doi.org/10.1016/j.ijimpeng.2009.05.006)

Reference: IE 1790

To appear in: *International Journal of Impact Engineering*



Please cite this article as: Jones N, Birch RS. Low-velocity impact of pressurised pipelines, *International Journal of Impact Engineering* (2009), doi: 10.1016/j.ijimpeng.2009.05.006

This is a PDF file of an unedited manuscript that has been accepted for publication. As a service to our customers we are providing this early version of the manuscript. The manuscript will undergo copyediting, typesetting, and review of the resulting proof before it is published in its final form. Please note that during the production process errors may be discovered which could affect the content, and all legal disclaimers that apply to the journal pertain.

**LOW-VELOCITY
IMPACT OF PRESSURISED PIPELINES**

Norman Jones* and R. S. Birch

**Impact Research Centre, Department of Engineering,
University of Liverpool, Liverpool L69 3GH.**

Corresponding author, e-mail: norman.jones@liv.ac.uk

ABSTRACT

Experimental tests are reported on steel pipelines which have been struck by a relatively large rigid wedge-shaped mass travelling up to 10.4 m/s. A pipeline is supported across a span, is fully clamped at both ends and is struck at the mid-span and at the one quarter span positions. Most of the pipelines are pressurised with a nitrogen gas. The initial impact energy produces large inelastic ductile deformations of the pipeline and, in some cases, failure.

A method is introduced which idealises a deformed pipeline cross-section in order to estimate the local and global components of the total displacement from experimental measurements of the final cross-section. Comparisons are also made with several previously published experimental studies for which sufficient data are available to make the calculations. A clearer insight into pipeline behaviour is achieved than is possible only with values of the maximum permanent transverse displacements which have been reported in previous experimental studies. This information should assist with pipeline design, provide more rigorous validation for numerical schemes and contribute to a better understanding of pipeline failure.

Recommendations are made on the accuracy and suitability of some well known empirical equations for predicting the permanent deformations of pressurised and empty pipelines caused by large rigid masses, relative to the pipeline mass, travelling with low initial impact velocities up to about 15 m/s.

Keywords: *pipelines, impact loading, internal pressure, ductile deformations, failure, empirical equations, geometrically similar scaling.*

NOTATION

p	internal pressure
r	rise, in the impact plane, of the distal surface of a pipeline, defined in Figure 6
r_o	radius of deformed cross-section, defined in Figure 5
D	outside diameter of a pipeline
D_m	defined in Figure 6
E_k	initial kinetic energy of a striker
G	mass of a striker
H	wall thickness of a pipeline
K	constant in the empirical analysis of Ellinas and Walker [17]
$2L$	span of a fully clamped pipeline
L_1	impact location of a striker measured from a clamped support, as shown in Figure 1.
R	mean radius of a pipeline
T_r	defined in Figure 6
V_0	initial impact velocity of a striker
W_f	maximum permanent transverse displacement of a pipeline
W_g, W_l	global and local displacements defined in Figure 6
W^*	$W/2R$

ε_r	engineering rupture strain of a uniaxial tensile test specimen cut from a pipeline
λ	$GV_o^2L/32\sigma_yR^2H^2$
ρ	density of the pipeline material
σ_y, σ_u	uniaxial yield stress and ultimate tensile strength of the pipeline material.
Δ^*	$W_l/2R$

1. INTRODUCTION

Many articles have been written on the impact behaviour of pipelines which are empty, filled with a variety of media, or pressurised, and some theoretical predictions and empirical equations are available for design purposes [1-3]. However, the number of variables controlling the behaviour of a pipeline is large, and those pipelines which have been studied, are made from different materials, have different support conditions and dimensions (diameter, thickness, span) and are struck at various locations across a span by missiles having different masses, geometries, and a wide range of initial impact velocities. In some cases, the pipelines have been filled with gases and materials having various degrees of compressibility at atmospheric pressure or pressurised. To complicate matters further, the response of a pipeline supported at discrete intervals and struck transversely on the span, consists of local indentations under the striker, together with a global beam-like behaviour, and stress waves, which might be generated within the pipe

wall and in any contents. Moreover, several different criteria for failure have been used by various authors.

Indenters, impactors, strikers or missiles having wedge, conical, spherical and blunt shaped impact faces have been used in experimental tests, and can give rise to different failure modes, as is well known for the impact perforation of flat plates. For example, the wedge shaped impactors in Reference [4] do not perforate a pipeline, but either cause a localised cracking behaviour with a slow leakage of the pressurised contents underneath the impactor (mode 1), or cause a global failure at one or both supports with a catastrophic release of the contents (mode 2). Other studies have examined the perforation of a tube wall by the impact of spherical missiles [3]. The pipeline material might be almost strain rate insensitive (e.g., aluminium alloys), or strongly strain rate sensitive (e.g., mild steel), and this phenomenon might be more significant at higher impact velocities and less important, but not negligible, at lower impact velocities, which are often taken as quasi-static.

Any contents of a pipeline would provide an inertial resistance to the deformation of a pipeline wall through the phenomenon of an “added mass” effect. The effect of this phenomenon increases as the density of the contents is increased, and is in addition to the inertial resistance of the pipeline wall material.

This plethora of variables is responsible for several authors reaching conclusions from their work which appear to conflict with the results of earlier studies on filled pipelines. In any event, the experimental investigations in References [4-12] all find that the addition of any contents in a pipeline (liquid, gas or granular), whether pressurised or not, causes smaller deformations to develop in the vicinity of the impact site when

compared with the behaviour of similar empty tubes, i.e., the deformation profile becomes more localised. This localisation of the damaged area is due likely to the additional inertial resistance offered by the contents of a pipeline. Thus, the impact energy is absorbed in a smaller volume of the tube material which is responsible for a decrease in the perforation energy, as observed in References [4, 7-10, 12]. Moreover, the experimental studies reported in References [4, 7-10, 12] indicate that an increase in the internal pressure does not produce any important further change in the response, which, perhaps, suggests that the density of the contents is the most significant parameter. Indeed, Reference [8] has shown that a 10 per cent reduction in the energy of a conical striker is associated with the cracking of a pipeline which is filled with water ($\rho = 10^3 \text{ kg/m}^3$) at atmospheric pressure, when compared with that for an empty tube. Similarly, a 20 per cent reduction occurs for a Woods metal filling having a density of $\rho = 10^4 \text{ kg/m}^3$. Moreover, the studies [4] with a nitrogen gas pressure also show only a small reduction in the perforation energies for a local failure, although the effect is significant for global failures, particularly when pipelines are struck at the mid-span. Schwer et al [11] also observed that internal pressures giving hoop stresses up to at least $2\sigma_y/3$, approximately, had little effect on the impulse required to burst a shell, although the deformation pattern was changed. It was observed in Reference [4] that the velocity for the onset of a global failure of mild steel pipes did reduce with an increase in an internal gas pressure in contrast to the local failure. Nishida and Tanaka [9] found that the response of aluminium 6063 T3 and aluminium 6063 H18 tubes, impacted by spherical missiles with masses up to 3.52 g and travelling up to 200 m/s, did agree with the general observation made above that the ballistic velocity was reduced by the addition of water in

the pipeline. In contrast to the above general observations, and to the results of Reference [9], Ma Xiaoqing and Stronge [5] have observed that the ballistic limit increased with an increase of the density of the contents (water and sand) in mild steel tubes. The tubes were struck by spherical missiles weighing up to 8.35 g and travelling up to 427 m/s. The only significant differences between these two sets of tests is the fact that Reference [5] studied mild steel tubes, which have a density which is about 2.9 times greater than the density of the aluminium alloy tubes in Reference [9], in addition to which, the flow stress of the mild steel material has an enhanced sensitivity to the strain rate. Is the enhancement of the ballistic velocity in Reference [5] due to the inertial resistance of the mild steel tubes and/or the important material strain rate effects for mild steel at the higher initial impact velocities in these two studies?

Palmer et. al. [13] have estimated strain rates of 0.3 to 4.6 s⁻¹ in eight tests on concrete-coated pipelines impacted at velocities between 5.91 and 8.23 m/s. The pipeline wall curvatures in the longitudinal directions were calculated from the final internal radial displacement profiles of the pipelines and used to estimate strains of 0.002 to 0.067. The strain rate was then estimated when dividing these values by the recorded response duration for each test specimen. Palmer et. al. [13] examined the influence of material strain rate sensitivity with the Cowper Symonds equation [14] having the usual coefficients for the yield stress of mild steel ($D = 40.4 \text{ s}^{-1}$, $q = 5$). It was estimated that the dynamic yield stresses are 1.37 to 1.65 times the static yield stresses for the eight test specimens.

Now returning to the studies in References [5, 9], it is noted that the strains in the pipeline specimens are larger than those in the specimens in Reference [13] because of

the damage sustained which includes perforation. The constants in the Cowper Symonds equation depend on various characteristics of the material and, ideally, they should be obtained from dynamic tests on the actual pipeline material. Moreover, the values of the constants vary with the magnitude of the plastic strain [15], the value of D, for example, being much larger for the ultimate tensile stress of mild steel when compared with the value for the corresponding yield stress. The values of the constants quoted in the literature for aluminium alloys are also widely different [14].

If it is assumed that $D = 1300 \text{ s}^{-1}$ and $q = 5$ for mild steel at a uniaxial tensile strain of 0.05 [15] and $D = 1288000 \text{ s}^{-1}$ and $q = 4$ for aluminium alloy [14], then the ratio between the strain rate enhancement for mild steel and aluminium alloy pipelines is

$$\frac{1 + (\dot{\epsilon}/1300)^{1/5}}{1 + (\dot{\epsilon}/1.288 \times 10^6)^{1/4}},$$

approximately. This ratio gives 1.20, 1.31 and 1.46 for strain rates of 1, 10 and 100 s^{-1} , respectively. In other words, the dynamic flow stresses of the mild steel are estimated to be of order 20 to 46 per cent greater, than those for the aluminium alloy, depending on the actual strain rate. Clearly, this is a significant effect and could be responsible for the ballistic limit in Reference [5] increasing with an increase in the density of the pipeline contents, whereas it decreases in Reference [9], and in other studies.

The present manuscript extends the study in Reference [4] by reporting some additional experimental results on the low-velocity impact behaviour of steel pipelines pressurised with a nitrogen gas. The local and global components of the total transverse

permanent displacement are calculated from the experimental test results using a method developed in Reference [2] and discussed further in this paper. They are presented for the current test results as well as for four previous experimental studies [4, 7, 16, 21]. The accuracy of the predictions of several empirical equations for the local, global and total displacements is also explored in this manuscript.

2. EXPERIMENTAL DETAILS

The experimental arrangement used for the current tests is similar to that illustrated in Figure 1 of Reference [4] and is idealised in Figure 1 here. The pipeline has a mean radius $R = 14.5$ mm, a thickness $H = 1$ mm and is fully clamped in a fitting which is mounted on the anvil of a drop hammer rig. The free span of all of the pipelines is $2L = 300$ mm and they are pressurised through the end clamps with a nitrogen gas. The wedge-shaped missile has a mass G with an included angle of 15 degrees and has the same shape as that used in Reference [4]. The impact face is 30 mm wide and 1.5 mm across with the 30 mm width orthogonal to the pipeline axis. The test specimens are made from cold-drawn mild steel pipes which are struck transversely at the mid-span and one-quarter span locations. Static uniaxial mechanical tests were conducted on the pipeline material in the axial direction giving a yield stress (σ_y) of 557 MPa, an ultimate tensile stress (σ_u) of 589 MPa and an engineering rupture strain of 0.06.

The impact loads are sufficient to cause large ductile deformations (D) of a pipeline, as indicated in Figures 2 and 3(a), without any leakage of the internal pressure. However, for sufficiently large impact energies, then failure of a pipeline allows the pressurised contents to escape. Two major failure modes have been identified as modes 1 and 2 in Reference [4]. Mode 1 is a local failure caused by a crack which develops in the pipeline wall immediately underneath the striking edge of a wedge-shaped missile, as indicated in Figure 3(b). Generally speaking, at the threshold energy, the internal pressure commences to leak slowly out of the pipeline when the missile is removed from the pipeline. This response occurs due to an elastic unloading of the stresses from a deformed plastic state which allows a crack to open. Mode 2 occurs in the pipeline wall near to a clamped support and is often catastrophic because it can release suddenly the internal pressure, as indicated in Figure 3(c).

The experimental data for the current tests are presented in Tables 1 and 2 for impacts at the mid-span and one-quarter span positions, respectively. Some further details on this test programme are given in Reference [12].

3. EMPIRICAL EQUATIONS FOR MAXIMUM PERMANENT TRANSVERSE DISPLACEMENT

Several empirical equations have been developed over the years for predicting the final permanent transverse displacements (W_f), or damage, of empty pipelines, as noted in References [1,4,16]. The predictions of [17-19] are given in Appendices 1 to 3 and compared in [2] with the experimental data reported in [16]. Ellinas and Walker [17] with $K = 150$ gave good agreement with the experimental data for pipelines with $2R/H = 30$

and 40 and struck at the mid-span. Soreide and Amdahl [19] predict good agreement for $2R/H = 11$ and 21, while de Oliveira et al [18] predict reasonable agreement with all of the experimental data which was recorded within the range $2R/H = 11$ to $2R/H = 60$. It was also found that the predictions of Ellinas and Walker [17] overpredicted W_f/H for a given value of $\lambda = (GV_o^2L/32\sigma_yR^2H^2)$ for the empty pipelines with $2R/H = 35.3$ reported in [4], while their estimates with $K = 300$ gave reasonable agreement with the experimental results.

The current test results for the maximum permanent transverse displacements of empty pipelines ($p = 0$) impacted at the mid-span are compared with the empirical equations of References [17-19] in Figure 2 of Reference [12]. It transpires that the theoretical predictions of Oliveira et al [18] with $L_1/L = 1$ and $pR/\sigma_yH = 0$, provides a reasonable estimate and predicts the general trend for the experimental data of Reference [4] and of Table 1 in Reference [12] and Table 1 here, while Soreide and Amdahl [19] provide a lower bound on the value of W_f/H for a given value of λ . Ellinas and Walker [17] with $K = 300$ over-predict W_f/H for the results having $L_1/L = 1$ and $pR/\sigma_yH = 0$ in Table 1 of [12] and Table 1 here. This equation does not predict the non-linear trend of the experimental results in the $W_f/H - \lambda$ space. Nevertheless, it gives good agreement with the results from [4] reported in Figure 2 of Reference [12].

It is evident from Figure 4 that References [18] and [19] again give reasonable predictions for the values of W_f/H from Table 1 here and References [4] and [12] when $p \neq 0$ and $L_1/L = 1$. Soreide and Amdahl [19] tend to predict more accurate values at the higher internal gas pressures, while de Oliveira et al [18] give better estimates for the lower internal pressures, so that these two empirical equations tend to bound the

experimental results in Figure 4, except, of course, for the global failures at one or both supports. However, neither equation specifically caters for the influence of internal pressure. Ellinas and Walker [17] do not retain the evident non-linearity of the experimental results in Figure 4, so with $K = 300$, and particularly with their recommended value of $K = 150$, the predictions, for a given value of λ , overestimate the value of W_f/H for the experimental results in Table 1 of Reference [12] and Table 1 here.

4. ESTIMATES FOR EXPERIMENTAL VALUES OF LOCAL AND GLOBAL DEFORMATIONS

The previous discussion on the pipeline deformations has been confined almost exclusively to the maximum permanent transverse displacements, W_f . However, it is evident from the photograph of a deformed pipeline in Figure 2 that the total displacement consists of local (i.e., squashing of the tube cross-section) and global (overall beam-like) displacements. In fact, several theoretical analyses have distinguished between the local and global displacements for the impact behaviour of pipelines, but it appears that experimental studies have reported only the overall permanent displacements and have not sought values for the two contributions. Additional recordings for each test specimen are required in order to obtain the two components, partly because of the complexity of the permanently deformed pipeline shape and the difficulty of establishing a datum for the global displacements. It is assumed in Reference [2] that the pipeline cross-section underneath the striker is deformed inextensionally in the circumferential

sense into a circular profile with a radius r_o and closed with a chord, as shown in Figures 5 and 6. Furthermore, the centre of the undeformed circular cross-section, which is used to define the global displacements, is assumed to coincide with the equal area axis of this deformed section. In this case, it is possible to obtain the local and global displacements from three measurements, viz., overall permanent displacement (W_f), local permanent thickness of deformed cross-section (T_r) and the maximum width of the deformed cross-section (D_m), which are shown in Figure 6. The analysis in Reference [2] can be rearranged to give the radius of the deformed section in Figure 5,

$$r_o = T_r \left\{ 1 + (D_m/2T_r)^2 \right\} / 2, \quad (1)$$

where T_r is the residual thickness across the deformed profile at the impact location and D_m is the maximum permanent width across the deformed section, as shown in Figure 6 for an idealised pipeline cross-section. Both of these quantities can be measured after an impact test.

The angles β and ϕ_o in Figure 5 are then given by

$$\beta = \pi R / 2r_o \quad (2)$$

and

$$\cos \phi_o = 1 - T_r / r_o. \quad (3)$$

The quantity δ in Figure 5 is

$$\delta = r_o (\cos \beta - \cos \phi_o), \quad (4)$$

which allows the local displacement to be estimated as

$$W_l = R - \delta \quad (5)$$

and the permanent global displacement is then

$$W_g = W_f - W_l, \quad (6)$$

where W_f is the maximum permanent transverse displacement at the impact location, as shown in Figure 6.

The maximum permanent transverse displacements (W_f) of the empty test specimens E in Reference [16], with $D/H = 30$ and struck at the mid-span, are compared in Figure 5(a) of Reference [4] with the empty test specimens in [4] having $D/H = 35.3$. It turns out that sufficient experimental data is reported in Reference [16] for pipeline specimens E to allow the displacements W_l and W_g to be calculated from equations (1) to (6) and presented in Figure 7. It is evident that the local displacements (W_l) are significant and are 0.58 to 0.97 times as large as the associated global displacements. The magnitude of the local displacement increases as the dimensionless initial kinetic energy (λ) increases, although, as a proportion of the total displacement, it tends to decrease.

The values of T_r , W_f and D_m have also been recorded for the current tests on pressurised and empty pipelines and are presented in Table 1. The local and global

displacements are estimated from equations (1) to (6) and plotted in Figure 7 for impacts at the mid-span. The local displacements (W_l) are 0.38 to 0.71 times the associated global displacements. Generally speaking, it is evident that the local displacements decrease with an increase in the internal pressure. The trend is less clear for the global displacements, though there appears to be a tendency for the global displacements to increase with an increase in the internal pressure, but it is not a strong trend. It also appears from these results that the critical value of λ for a pipeline failure decreases with an increase in the internal pressure.

The measurements D_m and T_r , which are defined in Figure 6, have been recorded for the pressurised pipeline test specimens reported in Reference [4]. This additional information, together with the data reported already for the impacted specimens, allows the local and global displacements to be estimated from equations (1) to (6). These results are presented in Table 3 and plotted in Figure 8. All specimens failed except one. A mode 1 failure, shown in Figure 3(b), occurred for the empty pipelines ($p = 0$) and the pipelines pressurised at $p = 66.3$ bar, while a mode 2 failure (see Figure 3(c)) predominates at the higher internal pressures of 99.3 bar and 132.7 bar. It is evident that the ratio W_l/W_g decreases as the internal pressure is increased so that $W_l > W_g$ for the empty pipelines, $W_l \cong W_g$ for an internal pressure of 66.3 bar, while the global displacements were larger than the local ones for higher pressures. Moreover, for a given value of the internal pressure, the ratio W_l/W_g tends to decrease as the dimensionless initial impact energy, λ , increases..

The theoretical analysis for the impact behaviour of the empty pipelines in Reference [2] caters for both the local and global displacements, but the numerical results have been

presented only for the total displacements and not the individual local and global contributions, although an examination of the deformed profile in Figure 16 in [2] indicates the presence of a substantial local component in a particular empty pipeline struck at the mid-span.

5. EMPIRICAL EQUATIONS FOR LOCAL DEFORMATIONS

Ellinas and Walker [17] presented an approximate theoretical analysis for the impact loading at the mid-span of fully clamped empty pipelines (see Appendix 1). The local permanent transverse displacement underneath a striker can be written in the form

$$\frac{W_1}{H} = \left(\frac{R}{H} \right) \left\{ \frac{96\lambda R\sqrt{2}}{KL} \right\}^{2/3} \quad (7)$$

with an empirical factor K which was taken as $K = 150$ in Reference [17]. However, according to equation (1.2) in Appendix 1, equation (7) with $K = 150$ is valid only up to $W_1/H = 5.8$, or $\lambda = 2.9$, when the local displacements cease and the global displacements commence for the pipelines in Table 1, as indicated in Figure 7. It is evident that the saturated value of the local displacement of $W_1/H = 5.8$ is almost one-half the corresponding experimental values for $p = 0$. It provides a better estimate for the local displacements of the pipelines containing the highest internal pressure of 150 bar in Table1.

Equation (7) requires a doubling of the factor K suggested by Ellinas and Walker [17], i.e., $K \cong 300$, in order to predict reasonable agreement with the values of the local displacements according to equations (1) to (6) for the experimental results from Reference [16] with $p = 0$, which are also plotted in Figure 7. As noted above, equation (7) has a limitation on the maximum value of W_l when the local displacements cease and the global displacements commence. However, the experimental results in Figure 7 do not show that the local displacements become saturated, or constant, above a particular value of λ , particularly for the results from [16], although more experimental study is required.

The local displacements which were calculated using equation (7) with $K = 150$ are in reasonable agreement with those for the empty pipelines having the same values of λ which were tested in Reference [4] and reported in Table 3 here and in Figure 8. The predictions are significantly greater than the corresponding experimental values for the pressurised pipelines, except for the largest values of the dimensionless impact energy, λ , in Figure 8. A constant factor $K = 300$ in equation (7) predicts local displacements which are about 25 per cent larger than those for $p = 0$. If the approximation $\beta \cong \left(\overline{\Delta^*}\right)^{1/2}$ for thin-walled pipelines is used instead of the more accurate expression for β in Reference [17] (see equation (1.3) in Appendix 1), then it turns out that the dimensionless local displacements become saturated when $W_f/H = 8.2$ and 3.0 for $K = 150$ and 300 , respectively. Although there are not many experimental results in Table 3 and in Figure 8, it is evident that the saturated value is close to the experimental values

for $K = 150$, but is much lower when $K = 300$. The corresponding values of λ calculated from equation (7) with $K = 300$ and $K = 150$ are 3.8 and 1.6, respectively.

Oliveira et al [18] have also produced a theoretical method for predicting the displacements of fully clamped empty pipelines, which are struck at the mid-span, and predicted that the permanent local displacements are given by (see Appendix 2)

$$\frac{W_1}{H} = \left(\frac{6R^2\lambda}{LH\sqrt{\pi}} \right)^{2/3} \quad (8)$$

which cease growing at a value

$$\frac{W_1^*}{H} = 4 \frac{R}{H} \left\{ k - (k^2 - 1)^{1/2} \right\}, \quad (9)$$

where

$$k = 1 + (\pi/8)(H/R)(L/R)^2. \quad (10)$$

It transpires that equation (8) predicts similar values of W_1/H to those from equation (7) by Ellinas and Walker [17], with $K = 150$, for the pipelines studied in this paper, as shown in Figure 7. However, equation (9) predicts that $W_1^*/H = 7.57$ when the local displacements cease growing for the empty pipelines in Figure 7. Most of the experimental values in Figure 7 are larger than this value and there appears to be no clear limiting, or saturated, value of the local displacement, which is contrary to the theory in

Reference [18], although there is a tendency for the local displacements (for $p = 0$) towards an asymptote. It should be noted from geometrical considerations alone that the maximum possible value of the local displacement is $W_1 \cong 2R$, or $W_1/H \cong 29$ for all of the pipeline test specimens in Figure 7.

Equation (8) respectively predicts $W_1/H = 13.5, 15.9$ and 19.0 for the pipelines NP9, NP3 and NP2 in Table 3 and Figure 8 when using the corresponding experimental values for the dimensionless impact energy λ . These dimensionless local displacements are 8.8, 4.6 and 11.7 per cent larger than the corresponding experimental values for $p = 0$. Thus, equation (8) provides a useful estimate for the local displacements of the empty pipelines studied in Reference [4], as shown in Figure 8. Nevertheless, equation (9) predicts that the local displacements become saturated at $W_1^*/H = 10.2$, or $\lambda = 5.8$, which is significantly smaller than all of the experimental results in Figure 8.

The local displacement (W_1) is smaller than $D - T_r$ due to the rise (r) of the distal surface of the pipeline in the impact plane, as shown in Figure 6 for the idealised deformed cross-section and in Figure 2 for an actual pipeline. This rise can be expressed in the form $r = D - (W_1 + T_r)$ and is significant compared to the corresponding local displacement. For example, the specimens B4 and B7 (see Figure 2) struck at the mid-span and with $p = 0$ have $r/W_1 = 0.27$, while $r/W_1 = 0.18$ for the pressurised specimens B18, B19 and B24. The ratio $r/W_1 = 0.31$ for the unpressurised specimens B8 and B9 struck at the one-quarter span position, while $r/W_1 = 0.22$ for the pressurised specimens B13 and B15. The test specimens E2 to E7 from Reference [16] with $p = 0$ and struck at the mid-span have ratios $r/W_1 = 0.21$ and 0.22 , while specimens E1 and E8 have ratios of 0.27 and 0.23 , respectively.

6. EMPIRICAL EQUATIONS FOR GLOBAL DISPLACEMENTS

The global displacements in Figure 7, which are predicted by Ellinas and Walker [17] with $K = 150$ (see equations (1.5) and (1.6) in Appendix 1), lie significantly above the corresponding experimental data from Table 1. Thus, the total permanent transverse displacements $W_{\bar{t}}/H = W_l/H + W_g/H$ would overpredict the experimental values for the pipelines, as could be seen by adding the two contributions in Figure 7 and as shown in Figure 4. The predictions of Reference [17] for the total displacements are compared with the experimental results from [16] in Figure 17 of [2] and in Figure 12 of [4].

It is evident from Figure 7 that the global displacements predicted by de Oliveira et al [18] (see equations (2.4) and (2.6) in Appendix 2) lie above the corresponding experimental values from Table 1. A combination of the underprediction of the local displacements, particularly for the empty pipelines, and the overprediction of the global displacements, gives total maximum permanent transverse displacements which are only slightly above the corresponding experimental values in Table 1, as indicated in Figure 4.

The empirical analysis of Ellinas and Walker [17] with $K = 150$ greatly exceeds the experimental values for the global displacements of the empty pipelines in Figure 8. On the other hand, the predictions of de Oliveira et al [18] are more reasonable for all values of λ , especially for the pressurised pipelines from Table 3 and Reference [4]. It is evident from Figure 8 that both the empirical equations from References [17] and [18] overpredict the corresponding experimental values, except for those pressurised pipelines which suffered a mode 2 failure.

Soreide and Amdahl [19] did not consider local deformations in their empirical equation since they assumed that all deformations were global ones. The maximum permanent transverse displacements, W_f , according to Soreide and Amdahl [19] (see Appendix 3) are presented in Figure 8 for the test pipelines in Table 3. The predictions are somewhat lower than the corresponding experimental values for the empty pipelines so that the predictions of References [18] and [19] provide approximate bounds on the maximum permanent transverse displacements. The comparisons made in Figure 17(a-e) of Reference [2] reveal that Soreide and Amdahl's predictions for W_f are generally too low for empty pipelines struck at the mid-span. Soreide and Amdahl predict reasonable agreement with the pressurised pipelines in Figure 8, except for those pipelines which suffer a mode 2 failure at the higher values of the dimensionless impact energy, λ .

7. IMPACTS AT ONE QUARTER SPAN POSITION

Unfortunately, most of the pipelines impacted at the one-quarter span position sheared off at a support, as indicated in Table 2, and so the results are less reliable than those in Table 1. The empty pipeline specimen B9 suffered only large ductile deformations and had a local displacement which is slightly larger than the associated global value. However, as λ increases (B8, B10) for $p = 0$, the local displacement decreases relative to the global displacement (0.92, 0.75). The pipeline specimens B13 and B14 have an internal pressure $p = 100$ bar and, for similar values of λ , the absolute values of the local displacements are smaller than those for the corresponding $p = 0$ case and are a significantly smaller proportion of W_g (0.56, 0.53). The pipeline specimens B15

to B17 have an internal pressure $p = 150$ bar and W_1 is an even smaller proportion of W_g (0.32-0.50). Again, as observed from Figure 7 for the mid-span impacts, it appears that as the internal pressure p increases, pipeline failure occurs for smaller values of λ .

Figure 9 has been plotted from the results in Table 4 which has been obtained using equations (1) to (6) and measurements recorded on the pipeline test specimens reported in Reference [4] and struck with a mass at the one-quarter span location. It is evident for a given value of the internal pressure that, despite the variety of failure modes, there is a tendency for the ratio W_1/W_g to decrease as λ increases. It is noteworthy for all of these test specimens and the range of λ studied that the local displacements are larger than the corresponding global ones.

8. DEFORMATIONS OF PIPELINES STUDIED IN REFERENCES [7] AND [21].

(a) Estimates for experimental values of local and global deformations.

The method outlined earlier was used to obtain the local and global displacements in Figures 7 to 9 for the current test results reported in Tables 1 and 2 and the related ones in Tables 3 and 4. This procedure is now used to obtain the components of the total displacements for the pipeline impact test results reported in References [7] and [21].

Chen and Shen [7] studied the ductile response and failure of fully clamped and pressurised mild steel pipelines impacted laterally at the mid-span by a wedge-shaped impactor with initial velocities up to 5.52 m/s. The experimental arrangement is similar to that used in References [4, 12 and 16], except that the pipelines were pressurised with

water. The authors give sufficient experimental data so that equations (1) to (6) can be used to calculate the local and global displacements which are presented in Figures 10 and 11. The trends of the local displacements for the pipelines pressurised with water are fairly consistent and have, possibly, reached a saturated value whether or not they have cracked, which is unlike the data for the internal gas pressures in Figures 7 and 8. The unpressurised (empty) pipelines have higher associated values of W_1 in both Figures 10 and 11. It appears that the local displacements tend to decrease as the internal water pressure is increased, which is also observed in Figures 7 and 8 for an internal nitrogen gas pressure.

The global displacements in Figures 10 and 11 increase with the dimensionless initial kinetic energy, λ . They have a tendency to increase with an increase in the internal water pressures for a given value of λ , whereas the unpressurised (empty) pipelines have distinctly lower values, which is particularly noticeable in Figure 11. Thus, the ratios of W_1/W_g are 0.32 ($p = 193$ bar) to 0.50 ($p = 86.2$ bar) and 0.30 ($p = 193$ bar) to 0.43 ($p = 86.2$ bar) in Figures 10 and 11, respectively, while the unpressurised (empty) pipelines have ratios of $W_1/W_g = 0.47$ in Figure 10 and $W_1/W_g = 0.59$ and 0.70 in Figure 11.

It is evident that the experimental values for the total displacements of the pipelines follow the same trend in Figures 10 and 11 regardless of whether or not they are pressurised with water. There is a tendency for the total permanent transverse displacements at a given value of λ to be slightly lower for the higher pressures in Figure 10, though this trend is less clear in Figure 11. The pressurised pipelines in Figures 10 and 11 fail at lower values of λ than the empty pipelines. Failure is considered to occur when a pipeline cracks.

Ng and Shen [21] have studied the behaviour of clamped cold drawn seamless steel pipelines pressurised with a nitrogen gas and struck at the mid-span by a rigid wedge-shaped mass. Their main interest focussed on the influence of a foundation which supported the underneath of a pipeline, but one series of test results was obtained without a foundation. Although only the maximum total permanent transverse displacements were presented in the paper, it turns out that sufficient information was recorded to calculate the local and the global components in Figure 12 from equations (1) to (6). The local, global and total displacements increase with an increase in λ and there is a tendency for the global and total displacements to increase with an increase in the internal pressure for a given value of λ . The local displacements for the pressurised pipelines are smaller than those for the empty ones. The average ratios of W_l/W_g range from 0.72 for $p = 0$ to 0.37 when $p = 125$ bar for the ductile deformations of the pipelines without any cracking. It is evident that there is a definite trend for the magnitude of λ associated with failure to decrease in Figure 12 as the internal pressure increases.

(b) Empirical equations for local displacements.

The predictions of the empirical equations (7) and (8), which were developed for $p = 0$, are given in Figures 10 and 11. The threshold values of λ , which correspond to the saturated values of the local displacements, are well below the experimental values reported by Chen and Shen [7]. Nevertheless, it is evident that the associated values of the dimensionless local displacements, W_l/H , both lie below the experimental results for

unpressurised (empty) pipelines, but do provide reasonable bounds for the pipelines pressurised with water, particularly for those in Figure 10.

The predictions of equations (7) and (8) are given in Figure 12 and are compared with the local displacements calculated from equations (1) to (6) using the experimental data presented by Ng and Shen [21]. The experimental results for $p = 0$ lie above both empirical predictions, while all of the values for the pressurised pipelines lie below. The threshold values of λ for the cessation of local deformations according to equation (1.4) and equation (9) are 3.9 and 5.9, respectively, which lie well below the smallest values in the experimental tests.

(c) Empirical equations for global and total displacements

The empirical equations (for $p = 0$) from References [17] (with $K = 150$) and [18] (see Appendices 1 and 2) predict global displacements (W_g) which are much higher than the corresponding experimental values for pipelines pressurised with water in Figures 10 and 11. Thus, they both overpredict the maximum permanent transverse displacements (W_f). However, the empirical equations predict global displacements which are lower than the experimental data for pipelines pressurised with a nitrogen gas in Figure 12, particularly for the predictions from Reference [18]. This behaviour contrasts with that observed in Figures 10 and 11. It is due likely to the axial movement of a pipeline within the supports during the experimental tests reported in Reference [21] which would give rise to larger transverse displacements.

Soreide and Amdahl's [19] empirical equations for the $p = 0$ case predict reasonable values for the maximum permanent transverse displacements (W_f) of the pipelines pressurised with water in Figures 10 and 11. The predictions are slightly above and below the corresponding experimental results in Figures 10 and 11, respectively, but would provide excellent design estimates for the pressurised or unpressurised (empty) pipelines studied in Reference [7]. However, this empirical equation underpredicts significantly the experimental data for W_f from Reference [21] in Figure 12 which is due likely to the axial movement which occurs at the pipeline supports during the tests.

9. DISCUSSION

It is evident from the new experimental results in Table 1 and those in References [4, 7, 12, 16, 21], Table 3 and Figures 7, 8 and 10-12 for the mid-span impacts of ductile pipelines, that the ratio W_l/W_g of the local and global displacements of pipelines calculated according to equations (1) to (6) generally decreases as the pressure p increases for a given value of the dimensionless impact energy λ . The ratio W_l/W_g decreases as λ increases for a given value of the internal pressure p . It is also observed from the results that the values of λ for the failure threshold of a pipeline decreases as the internal pressure increases. In most cases, this failure develops at a support (see Figure 3(c)) which appears to be a consequence of an increase in the global displacements relative to the local ones (i.e., W_l/W_g decreases). In other words, as the internal pressure increases, more impact energy is likely to be absorbed in an overall or global deformation mode at the expense of the local energy absorption underneath a striker. This

phenomenon is illustrated in Table 3 in which the mode 1 local failure (see Figure 3(b)) gives way to a mode 2 failure at one or both supports (see Figure 3(c)) as the dimensionless impact energy, λ , is increased at the higher internal pressures. The corresponding ratios of W_I/W_g decrease. This phenomenon is also evident in Table 1 where a large ductile deformation response (D) (see Figure 3(a)) gives way to a failure at a support (2) as λ increases; these threshold values of λ decrease as the internal pressure increases.

The ratios W_I/W_g are largest for the empty pipelines and exceed unity for some of those reported in Figure 8. The ratio W_I/W_g is smaller than unity for all of the pressurised pipelines reported in this paper except for the pipelines in Table 3 having $p = 66.3$ bar. Incidentally, the ratios p/p_y , where $p_y = \sigma_y H/R$, are fairly similar for all of the experimental results reported. The ratios p/p_y for the pressurised pipelines are 0.26 and 0.39 in Table 1; 0.16, 0.24 and 0.32 in Reference [4] and Table 3; 0.17, 0.24 and 0.37 in Reference [7] and Figure 10; 0.19, 0.34 and 0.42 in Reference [7] and Figure 11; 0.14, 0.21 and 0.28 in Figure 12.

Generally speaking, the maximum permanent total displacements (W_f) are bounded by the empirical predictions of de Oliveira et al [18] and Soreide and Amdahl [19] which were developed for empty pipelines. Reference [18] tends to predict high values of W_f while the values from Reference [19] are slightly low in most cases.

The threshold values of λ when the local displacements become saturated, as defined in Appendices 1 and 2, are generally much lower than any of the values of λ used in the experimental tests. However, the corresponding saturated values of W_I/H from Reference [17] (equation (1.2) in Appendix 1) and Reference [18] (equation (2.2) in Appendix 2)

give reasonable predictions for the corresponding experimental results in some cases (e.g., Figures 10 and 11 for an internal water pressure), but the experimental results for an internal nitrogen gas pressure show a continuous increase with λ (see Figures 7 and 8).

The empirical predictions of References [17] and [18] for the global displacements (W_g) are too high compared with the experimental data recorded on pipelines having an internal nitrogen gas pressure in Figure 7, and for the pipelines pressurised with water in Figures 10 and 11. De Oliveira et al [18] give reasonable agreement with the global displacements obtained from equations (1) to (6) for the pipelines in Figure 8, which were pressurised with a nitrogen gas.

The comparisons between the empirical equations and the experimental values in Figure 12, which were calculated from the data in Reference [21], reveal the important influence of the support conditions (see section 8(c)) because the trends are different to those observed in the other figures for pipelines with fully clamped supports having a more complete axial restraint.

The impact response of pipelines involves many parameters, only a limited range of which has been examined in the study reported here. For example, the pipeline geometry is described by several variables (R , H , L), as well as the support conditions, the impact location (L_1) and the static (σ_y , σ_u , ϵ_r) and dynamic properties of the pipeline material. The impact face of a striker can have many different shapes, though in the present study they all have a wedge shape. Other parameters include the magnitude of the internal pressure (p) and the pressurising medium as well as the range of the impact masses (G) and impact velocities (V_o). To examine systematically all of these effects would require a large experimental programme. Numerical schemes have been reported in References

[2] and [20] and can be used to examine the influence of various factors. For preliminary design purposes, and for the range of variables studied, some support has been offered here for the well known empirical equations. These equations were developed for empty pipelines, but an internal pressure does not have a major effect on the maximum permanent transverse displacements of a pipeline. However, an internal pressure does have an important role in causing a failure to develop at a support due to its influence on the deformation profile since the internal pressure changes the ratio of the local to global displacements.

It is found in Reference [12] that the maximum permanent transverse ductile displacement produced by an impact on pressurised pipelines might satisfy, approximately, the laws of geometrically similar scaling, but this cannot be shown conclusively because the range of experimental data does not lie within the range of data in a previous study [4] on larger diameter pipelines. However, a possible contributory factor why the range of data for the small-scale pipelines lies above that in [4] for the larger scaled pipelines is the observation that the impact energy producing a pipeline failure, which releases the gas pressure, does not satisfy the laws of geometrically similar scaling. It has been observed that the dynamic inelastic failure of a full-scale structural member occurs at roughly one half the scaled initial impact energy, which would have been expected from the scaled experimental results obtained using a one half scale model [14]. The observations on the scaled pipelines in Reference [12] confirm this observation.

Ng and Shen [21] reported some experimental results on the dynamic inelastic response and failure of mild steel pipelines struck with initial impact velocities up to 7.70 m/s at the mid-span. Some of the pipelines were supported along the entire span on sand

or kaolin foundations and were pressurised internally with a nitrogen gas which caused initial hoop stresses up to 27 per cent (125 bar) of the associated hoop yield strength. A finite-element analysis was also reported. The support foundations of pipelines have not been examined in this paper, so an interested reader is referred to Reference [21] for further details.

10. CONCLUSIONS

It is evident from the present results on steel pipelines that an increase in the dimensionless internal gas pressure (p/p_y , where $p_y = \sigma_y H/R$) up to about 0.4 only causes a small reduction in the maximum permanent transverse ductile displacement (W_f) for a given value of the impact energy, but it does cause an important reduction in the impact energy for failure.

The maximum permanent transverse ductile displacement of a pipeline struck at the one quarter span position is smaller than the corresponding value associated with a pipeline struck at the mid-span by a missile having the same initial impact energy. Moreover, failure occurs at smaller impact energies. These observations are consistent with impact studies on ductile metal beams struck at various locations across the span [22,23].

Some equations have been established for an idealised deformed pipeline cross-section in order to calculate the local (W_l) and global (W_g) displacements from experimental measurements of the maximum permanent transverse displacement (W_f) and the maximum permanent width (D_m) and depth (T_r) of a pipeline cross-section struck

by a rigid wedge travelling with impact velocities up to about 15 m/s. It transpires that the ratio (W_l/W_g) of the local to the global displacements decreases as the internal pressure in a pipeline increases. Generally speaking, this decrease is driven largely by a reduction in the local displacement. The magnitude of the local displacement increases as the dimensionless initial impact energy increases, although as a proportion of the total displacement it tends to decrease. A clearer understanding of the pipeline behaviour is achieved than is possible from studies which report only the maximum permanent transverse displacements. This additional information should assist with the design of pipelines, provide more rigorous validations for numerical schemes and contribute to an improved understanding of pipeline failure.

The empirical equations for the maximum permanent transverse displacements (W_f) in References [17,18] also give predictions for the local (W_l) and global (W_g) displacements of an empty pipeline. Both methods predict that the local displacements become saturated at a certain value of the dimensionless impact energy, whereas the experimental evidence for this saturation is not clear, despite the fact that the experimental values for the impact energies are well above the corresponding threshold values. In some cases, both theories underpredict the local displacements, while in others they overpredict. Generally speaking, the two methods overpredict the global displacements, particularly those predicted by Reference [17], but the total displacements (W_f) are reasonably well approximated by Reference [18]. In fact, Reference [18] tends to provide a good estimate of the large permanent ductile deformations at the mid-span of both the unpressurised and the pressurised pipelines. Thus, this empirical equation could be used for design purposes, at least on the basis of the range of parameters examined in

the current study ($20 \leq 2R/H \leq 35$, $L/R \cong 10$ and large ratios of the impact mass to the pipeline mass, e.g., 50.1 for the experimental results in Tables 1 and 2). The predictions of Soreide and Amdahl [19] provide a lower bound on the maximum permanent transverse displacements (W_f) for the unpressurised case, but give a good estimate for the values associated with the higher internal gas pressures. The empirical method of Ellinas and Walker [17] overpredicts the maximum permanent displacement, though the equations are simple to use and do provide an upper bound for the current results.

The new experimental results on pipelines reported in Tables 1 and 2 and those in References [4, 12, 21] and in Tables 3 and 4 were pressurised with a nitrogen gas, whereas those in Reference [7] were pressurised with water. Unfortunately, it is not possible to make a clear distinction between the responses of pipelines pressurised with nitrogen gas or water. It appears, on the basis of this limited study, that the general behaviour is similar whether or not a pipeline is pressurised with gas or water. In view of the observations of the study reported in Reference [8] and the discussion in section 1, it is clear that further work is required in order to clarify the influence of different contents on the impact behaviour of a pressurised pipeline.

ACKNOWLEDGEMENTS

The authors wish to take this opportunity to thank the Impact Research Centre at the University of Liverpool for their cooperation, to Mr. P. McMullon and Mr. Jijimon Mathew for their assistance with the experimental work and to Mrs. J. Jones and Mrs. I. M. Arnot for their assistance with the preparation of this manuscript

REFERENCES

1. Reid, S. R., Goudie, K., Denting and bending of tubular beams under local loads, Structural Failure, Ed., T. Wierzbicki and N. Jones, Wiley-Interscience, John Wiley and Sons, New York, pp 331-364, 1989.
2. Jones, N., Shen, W. Q., A Theoretical Study of the Lateral Impact of Fully Clamped Pipelines, proceedings Institution of Mechanical Engineers, Vol. 206(E), pp 129-146, 1992.
3. Stronge, W. J., Impact and perforation of cylindrical shells by blunt missiles, Metal Forming and Impact Mechanics, Ed. S. R. Reid, Pergamon Press, pp 289-302, 1985.
4. Jones, N., Birch, R. S., Influence of Internal Pressure on the Impact Behaviour of Steel Pipelines, Transactions ASME, Journal of Pressure Vessel Technology, Vol. 118, No. 4, 464-471, 1996.
5. Ma, X., Stronge, W. J., Spherical missile impact and perforation of filled steel tubes, International Journal of Impact Engineering, Vol. 3, No. 1, 1-16, 1985.

6. Stronge, W. J., Impact on metal tubes: indentation and perforation, Structural Crashworthiness and Failure, Ed. N. Jones, and T. Wierzbicki, Elsevier Applied Science, London and New York, pp 165-188, 1993.
7. Chen, K., Shen, W. Q., Further experimental study on the failure of fully clamped steel pipes, International Journal of Impact Engineering, Vol. 21, No. 3, 177-202, 1998.
8. Palmer, A., Neilson, A., Sivadasan, S., Pipe perforation by medium-velocity impact, International Journal of Impact Engineering, Vol. 32, No. 7, 1145-1157, 2006.
9. Nishida, M., Tanaka, K., Experimental study of perforation and cracking of water-filled aluminium tubes impacted by steel spheres, International Journal of Impact Engineering, Vol. 32, No.12, 2000-2016, 2006.
10. Neilson, A. J., Howe, W. D., Garton, G. P., Impact resistance of mild steel tubes: an experimental study, UK Atomic Energy Authority Report AEEW-R 2125, Winfrith, June 1987.
11. Schwer, L. E., Holmes, B. S., Kirkpatrick, S. W., Response and failure of metal tanks from impulsive spot loading: experiments and calculations, International Journal of Solids and Structures, Vol. 24, 817-833, 1988.

12. Jones, N., Birch, R. S., Impact behaviour of pressurised pipelines, Structures under Shock and Impact X, Ed. N. Jones and C. A. Brebbia, Proceedings Tenth International Conference on Structures under Shock and Impact, The Algarve, Portugal, WIT Press and WIT Transactions of the Built Environment, Vol. 98, pp 219-228, 2008.
13. Palmer, A., Touhey, M., Holder, S., Anderson, M., Booth, S., Full-scale impact tests on pipelines, International Journal of Impact Engineering, Vol. 32, No. 8, 1267-1283, 2006.
14. Jones, N., Structural Impact, Cambridge University Press, 1997.
15. Jones, N., Some Comments on the Modelling of Material Properties for Dynamic Structural Plasticity, International Conference on the Mechanical Properties of Materials at High Rates of Strain, Oxford. Ed. J. Harding, Institute of Physics Conference Series No. 102, pp 435-445, 1989.
16. Jones, N., Birch, S. E., Birch, R. S., Zhu, L., Brown, M., An Experimental Study on the Lateral Impact of Fully Clamped Mild Steel Pipes, proceedings Institution of Mechanical Engineers, Vol. 206(E), pp 111-127, 1992.
17. Ellinas, C. P., Walker, A. C., Damage on offshore tubular bracing members. IABSE Colloquium on Ship Collisions with Bridges and Offshore Structures. Copenhagen, pp 253-261, 1983.

18. de Oliveira, J. G., Wierzbicki, T., Abramowicz, W., Plastic behaviour of tubular members under lateral concentrated loading. Det Norske Veritas Tech. Rep. 82-0708, 1982.
19. Soreide, T. H., Amdahl, J., Deformation characteristics of tubular members with reference to impact loads from collision and dropped objects, Norwegian Maritime Research Paper 2, pp 3-12, 1982.
20. Shen, W. Q., Shu, D. W., A theoretical analysis on the failure of unpressurised and pressurised pipelines, proceedings Institution of Mechanical Engineers, Vol. 216(E), pp 151-165, 2002.
21. Ng, C. S., Shen, W. Q., Effect of lateral impact loads on failure of pressurised pipelines supported by foundation, proceedings Institution of Mechanical Engineers, Vol. 220(E), pp 193-206, 2006.
22. Jones, N., Jones, C., Inelastic failure of fully clamped beams and circular plates under impact loading, proceedings Institution of Mechanical Engineers, Vol. 216(C), 133-149, 2002.
23. Alves, M., Jones, N., Impact failure of beams using damage mechanics: part 2-application, International Journal of Impact Engineering, Vol. 27, No. 8, 863-890, 2002.

No.	p (bar)	V _o (m/s)	λ	W _f (mm)	D _m (mm)	T _r (mm)	W _l (mm)	W _g (mm)	Failure mode
B4	0	9.36	37.6	32.0	40.4	14.0	12.6	19.4	2
B5	0	8.10	28.0	29.2	39.6	15.0	12.1	17.1	D
B6	0	8.74	32.8	31.6	40.0	14.1	12.7	18.9	D
B7	0	9.04	35.2	33.1	40.5	13.5	13.0	20.1	D
B18	100	9.34	37.6	36.8	36.8	17.7	10.4	26.4	2*
B19	100	8.10	28.0	26.1	35.3	20.1	8.4	17.7	D
B20	100	8.74	32.8	29.5	35.6	19.4	9.0	20.5	2
B21	100	8.43	30.4	28.0	35.6	19.7	8.7	19.3	2
B23	150	8.10	28.0	25.4	34.4	21.2	7.4	18.0	2
B24	150	8.74	32.8	30.4	35.3	19.9	8.6	21.8	2
B26	150	8.43	30.4	27.3	34.4	21.1	7.5	19.8	2
B27	150	7.75	25.6	21.5	33.5	22.4	6.2	15.3	D

Table 1. Experimental data for steel pipelines having $\sigma_y = 557$ MPa, $\sigma_u = 589$ MPa, $2R = 29$ mm, $2L = 300$ mm, $H = 1$ mm and struck at the mid-span with a mass $G = 10.75$ kg.

1: Failure at the impact point (mode 1); 2: failure at a clamped support (mode 2); D:

ductile behaviour with no failure; *: end completely sheared off from a support; W_f is estimated by taping the two parts together.

No.	p (bar)	V_o (m/s)	λ	W_f (mm)	D_m (mm)	T_r (mm)	W_l (mm)	W_g (mm)	Failure mode
B8	0	9.34	37.6	31.1	43.2	10.5	14.9	16.2	2
B9	0	8.08	28.0	25.9	41.8	12.6	13.2	12.7	D
B10	0	10.43	46.4	32.1	42.6	11.3	13.8	18.3	1,2
B13	100	8.10	28.0	29.9	38.4	16.9	10.7	19.2	2*
B14	100	10.43	46.4	31.5	38.8	16.6	10.9	20.6	2*
B15	150	9.34	37.6	30.7	38.0	17.7	10.1	20.6	2*
B16	150	10.43	46.4	51.0	41.8	13.9	12.3	38.7	2*
B17	150	8.10	28.0	29.1	37.7	18.2	9.7	19.4	2*

Table 2. Experimental data for steel pipelines struck at the one-quarter span with a mass $G = 10.75$ kg. The material properties, geometry and failure modes are defined in Table1.

No.	p (bar)	V _o (m/s)	λ	W _f (mm)	D _m (mm)	T _r (mm)	W _l (mm)	W _g (mm)	Failure mode
NP9	0	8.74	8.8	17.6	65.95	45.0	12.4	5.2	D
NP3	0	9.50	11.2	23.1	70.25	41.7	15.2	7.9	1
NP2	0	11.28	14.7	27.6	73.50	39.3	17.0	10.6	1
P04	66.3	8.74	8.8	15.1	59.75	50.0	7.8	7.3	1
P22	66.3	9.15	9.7	16.2	62.50	48.9	8.6	7.6	1
P03	66.3	9.85	11.2	18.6	64.90	47.8	9.5	9.1	1
P02	66.3	11.28	14.7	25.9	67.95	41.8	15.6	10.3	1
P23	99.3	9.50	10.4	17.0	62.25	49.1	8.4	8.6	1
P09	99.3	9.85	11.2	18.1	62.75	49.0	8.5	9.6	1
P20	99.3	10.57	12.9	30.4	66.70	43.9	13.5	16.9	2
P10	99.3	11.28	14.7	40.9	68.60	41.0	16.3	24.6	2
P34	132.7	9.50	10.4	21.1	62.60	47.8	9.9	11.2	2
P31	132.7	9.85	11.2	17.8	61.90	50.0	7.4	10.4	1
P33	132.7	10.57	12.9	29.6	64.95	44.8	12.9	16.7	2
P32	132.7	11.28	14.7	35.9	66.00	43.2	14.4	21.5	2

Table 3. Additional experimental data for steel pipelines struck at the mid-span and reported in Table 1 of Reference [4]. $2R = 58.3$ mm, $H = 1.7$ mm, $2L = 600$ mm and further details are found in Reference [4]. The failure modes are defined in Table 1.

No.	p (bar)	V_o (m/s)	λ	W_f (mm)	D_m (mm)	T_r (mm)	W_l (mm)	W_g (mm)	Failure mode
P26	66.3	9.50	10.4	22.6	66.1	43.8	13.7	8.9	1,2
P15	66.3	9.85	11.2	25.5	67.5	43.1	14.2	11.3	1,2
P16	66.3	11.28	14.7	32.0	71.7	39.8	16.9	15.1	1,2
P17	99.3	7.47	6.5	11.5	59.4	50.4	7.4	4.1	D
P25	99.3	8.07	7.5	12.5	60.7	50.2	7.4	5.1	1
P11	99.3	8.74	8.8	18.7	63.0	46.8	10.9	7.8	2
P29	132.7	7.47	6.5	10.8	58.8	51.5	6.2	4.6	1
P28	132.7	8.07	7.5	14.3	60.8	49.9	7.7	6.6	2
P27	132.7	8.74	8.8	17.1	61.9	48.1	9.7	7.4	2

Table 4. Additional experimental data for steel pipelines struck at the one-quarter span and reported in Table 2 of Reference [4]. $2R = 58.3$ mm, $H = 1.7$ mm, $2L = 600$ mm and further details are found in Reference [4]. The failure modes are defined in Table 1.

APPENDIX 1

THEORY OF ELLINAS AND WALKER [17]

The quasi-static theoretical procedure in Reference [17] is developed for a fully clamped rigid, perfectly plastic pipeline struck at the mid-span ($L_1 = L$) by a mass G travelling with an initial velocity V_0 , as shown in Figure 1. Both local and global deformations are retained in the analysis but the strengthening influence of axial membrane forces, or geometry changes, is neglected for the global deformations. The local deformations cease immediately when global behaviour commences.

The energy absorbed plastically during the local indentation phase is

$$E_1 = KRH^2\sigma_y(\Delta^*)^{3/2}/3, \quad 0 \leq \Delta^* \leq \bar{\Delta}^*, \quad (1.1)$$

where $K = 150$ and $\bar{\Delta}^*$ is the dimensionless indentation when global deformations commence, which is obtained from

$$\bar{\Delta}^* = \left\{ 32R^2(1 + \cos\beta - \beta)/KLH \right\}^2 \quad (1.2)$$

with

$$\beta = \left[1 - (2R/H) \left\{ \left(16\bar{\Delta}^{*2}/9 + (H/2R)^2 \right)^{1/2} - 4\bar{\Delta}^*/3 \right\} \right] \bar{\Delta}^{*1/2}. \quad (1.3)$$

If the kinetic energy of the striker in Figure 1 is not sufficient to activate the global deformation phase, then motion ceases during the local deformation phase and

$$\lambda = KL\bar{\Delta}^{*3/2}/48R, \quad 0 \leq \Delta^* \leq \bar{\Delta}^*, \quad (1.4)$$

where λ is the dimensionless initial kinetic energy. For a larger initial kinetic energy which produces $\Delta^* = \bar{\Delta}^*$ and $W^* > 0$, then the global energy absorbed is

$$E_g = 16HR^3\sigma_y(1 + \cos\beta - \beta)W^*/L. \quad (1.5)$$

Thus, equating the initial kinetic energy to the sum of the local and global plastic energy absorption gives

$$\lambda = KL\bar{\Delta}^{*3/2}/48R + R(1 + \cos\beta - \beta)W^*/H, \quad (1.6)$$

where $\Delta^* = \bar{\Delta}^*$ and $W^* \geq 0$.

APPENDIX 2

THEORY OF OLIVEIRA, WIERZBICKI AND ABRAMOWICZ [18]

The quasi-static theoretical procedure in Reference [18] is developed for a fully clamped rigid, perfectly plastic pipeline struck at the mid-span ($L_1 = L$) by a mass G travelling with an initial impact velocity V_0 , as shown in Figure 1. Both local and global deformations are studied in this theoretical analysis, and the influence of axial membrane forces, or geometry changes, is retained for the global deformations. However, the local deformations are assumed to cease immediately when the global behaviour commences.

The local denting behaviour absorbs the external energy

$$E_1 = 8\pi^{1/2}\sigma_y(HW_1)^{3/2}/3 \quad (2.1)$$

up to the dimensionless local deformation

$$\bar{\Delta}^* = 2\left\{k - (k^2 - 1)^{1/2}\right\}, \quad (2.2)$$

where

$$k = 1 + \pi H(L/R)^2/8R. \quad (2.3)$$

The local denting behaviour ceases and the global behaviour commences when $\Delta^* = \bar{\Delta}^*$. The energy absorbed plastically during this deformation phase is

$$E_{g1} = \left(16\sigma_y R^3 H/L\right) \left[\left(8/\pi^2\right) (1 - \bar{\Delta}^*) (2 - \bar{\Delta}^*) \sin\left\{\pi^2 W^* / \left(8(1 - \bar{\Delta}^*)\right)\right\} + \pi^2 W^{*3} / \left(12(1 - \bar{\Delta}^*)\right) \right] \quad (2.4)$$

so that the total energy absorbed by a pipeline is $E_t = E_l + E_{g1}$ until

$$W^* = \bar{W}^* = 4(1 - \bar{\Delta}^*)/\pi. \quad (2.5)$$

For global deformations larger than \bar{W}^* , the impact energy is absorbed by a pure membrane behaviour of a pipeline, or

$$E_{g2} = \left(8\pi\sigma_y R^3 H/L\right) (W^{*2} - \bar{W}^{*2}). \quad (2.6)$$

Thus, the total energy absorbed is $E_t = E_l + E_{g1} + E_{g2}$ which must be equated to the initial kinetic energy $GV_0^2/2$ when it is sufficiently large to generate deformations in all three phases.

APPENDIX 3

THEORY OF SOREIDE AND AMDAHL [19]

The quasi-static theoretical procedure in Reference [19] is developed for a fully clamped rigid, perfectly plastic pipeline struck at the mid-span ($L_1 = L$), as shown in Figure 1. The initial local indentation phase is neglected by Soreide and Amdahl, but geometry changes, or finite deflections, are retained during the global deformation phase with the pipeline retaining the original circular cross-section.

The initial kinetic energy of the striking mass in Figure 1 is equated to the energy absorbed plastically in a pipeline to give

$$GV_0^2 / 2 = 8\sigma_y R^3 H \left\{ 3W^* (1 - W^{*2})^{1/2} + (1 + 2W^{*2}) \sin^{-1}(W^*) \right\} / L, \quad 0 \leq W^* \leq 1, \quad (3.1)$$

or

$$\lambda = 1.5(R/H)W^* (1 - W^{*2})^{1/2} + (R/H)(W^{*2} + 0.5) \sin^{-1}(W^*), \quad 0 \leq W^* \leq 1. \quad (3.2)$$

Similarly,

$$\lambda = \pi R (1 + 2W^{*2}) / 4H, \quad W^* \geq 1. \quad (3.3)$$

LIST OF FIGURES

Figure 1. A mass G travelling with an initial velocity V_0 and striking a pipeline which is fully clamped across a span of $2L$.

Figure 2. Photograph of the permanently deformed pipeline specimen B7 (see Table 1).

Figure 3. Failure modes of a pipeline. (a) large ductile deformations (D), (b) mode 1, local failure, (c) mode 2, global failure.

Figure 4: Comparison between experimental results and empirical predictions for the dimensionless maximum permanent transverse displacement, W_f/H and the dimensionless initial impact energy (λ) of fully clamped pressurised ($p \neq 0$) steel pipelines struck at the mid-span ($L_1/L = 1$).

Experimental results: \blacklozenge , large ductile deformations (D) (Table 1 of [12] and Table 1 here); \blacklozenge , failure at a clamped support (mode 2) (Table 1 of [12] and Table 1 here); \blacktriangle , large ductile deformations (D) [4]; \blacktriangle , local failure at the struck position (mode 1) [4]; \square , global failure at a support (mode 2) [4]. The superscripts 1, 2 and 3 refer to $pR/\sigma_y H = 0, 0.26$ and 0.39 , respectively, for the specimens in Table 1 of [12] and Table 1 here. The superscripts 1, 2, 3 and 4 refer to $pR/\sigma_y H = 0, 0.16, 0.24$ and 0.32 , respectively, for the specimens [4].

Empirical predictions for the specimens in Table 1 of [12] and Table 1 here with $p = 0$: 1 and 2, Ellinas and Walker [17] with $K = 150$ and $K = 300$, respectively; 3, de Oliveira et al [18]; 4, Soreide and Amdahl [19].

Figure 5. Original and deformed cross-section of a pipeline in the impact plane.

Figure 6. Definitions of the local indentation (W_l), global displacement (W_g) and total displacement (W_f) for the idealised deformed cross-section of a pipeline.

Figure 7. Experimental values for the local (W_l), global (W_g) and total (W_f) permanent transverse displacements of fully clamped steel pipelines impacted at the mid-span (L_1/L

= 1) versus the dimensionless initial kinetic energy (λ). Results from Table 1 and Reference [16].

Experimental Results:

◆, ◇: W_f ; for large ductile deformations and failure at a clamped support, respectively.

●, ○: W_g ; for large ductile deformations and failure at a clamped support, respectively.

■, □: W_l ; for large ductile deformations and failure at a clamped support, respectively.

+ : W_f [16], series E, $p = 0$.

▼ : W_g [16], series E, $p = 0$.

▲ : W_l [16], series E, $p = 0$.

The superscripts 1, 2 and 3 refer to $p = 0, 100$ and 150 bar, respectively.

*: the pipeline was completely sheared off from a support; W_f is estimated by taping the two parts together.

Empirical equations for unpressurised pipelines in Table 1:

----- 1, ----- 1; W_l and W_g , Ellinas and Walker[17] with $K = 150$.

----- 3, ----- 3; W_l and W_g , de Oliveira et al [18].

Figure 8. Experimental values from Table 3 for the local (W_l), global (W_g) and total (W_f) permanent transverse displacements of fully clamped steel pipelines impacted at the mid-span ($L_1/L = 1$) [4] versus the dimensionless initial kinetic energy (λ).

◆, ●, ■: W_f , W_g and W_l for large ductile displacements, respectively.

◇, ○, □: W_f , W_g and W_l for a mode 1 failure, respectively.

+, ▼, ▲: W_f , W_g and W_l for a mode 2 failure, respectively.

The superscripts 1, 2 and 3 refer to $p = 66.3$ bar, $p = 99.3$ bar and $p = 132.7$ bar, respectively. The $p = 0$ case has no superscript.

Empirical equations for unpressurised pipelines in Table 3:

----- 1, ----- 1, — · — · — 1; W_l , W_g , W_f , Ellinas and Walker [17] ($K = 150$).

----- 3, ----- 3, — · — · — 3; W_l , W_g , W_f , de Oliveira et al [18].

————— 4; W_f , Soreide and Amdahl [19].

Figure 9. Experimental values from Table 4 for the local (W_l), global (W_g) and total (W_f) permanent transverse displacements of fully clamped steel pipelines impacted at the one-quarter span position ($L_1/L = 0.5$) [4] versus the dimensionless initial kinetic energy (λ). The notation is the same as defined in Figure 8.

Figure 10. Experimental values from equations (1-6) for the local (W_l), global (W_g) and total (W_f) permanent transverse displacements of fully clamped steel pipelines impacted at the mid-span ($L_1/L = 1$) (AP13 series) [7] versus the dimensionless initial kinetic energy (λ). $R = 9.05$ mm, $H = 0.9$ mm, $2L = 200$ mm and $G = 25.2$ kg.

◆, ●, ■: W_f , W_g and W_l for large ductile displacements, respectively.

◇, ○, □: W_f , W_g and W_l for a cracked pipeline, respectively.

The superscripts 1, 2 and 3 refer to internal water pressures of $p = 86.2$ bar, $p = 124$ bar and $p = 193$ bar, respectively. The $p = 0$ case has no superscript.

Empirical equations for the unpressurised pipelines in Reference [7] are defined in Figure 8.

Figure 11. Experimental values from equations (1-6) for the local (W_l), global (W_g) and total (W_f) permanent transverse displacements of fully clamped steel pipelines impacted at the mid-span ($L_1/L = 1$) (BP23 series) [7] versus the dimensionless initial kinetic energy (λ). $R = 18.2$ mm, $H = 1.6$ mm, $2L = 400$ mm and $G = 32.2$ kg.

The notation is the same as in Figure 10, except that the superscripts 1, 2 and 3 refer to internal water pressures of $p = 86.2$ bar, $p = 155$ bar and $p = 193$ bar, respectively. The $p = 0$ case has no superscript.

Figure 12. Experimental values from equations (1-6) for the local (W_l), global (W_g) and total (W_f) permanent transverse displacements of clamped steel pipelines impacted at the mid-span ($L_1/L = 1$) [21] versus the dimensionless initial kinetic energy (λ). $R = 27.7$ mm, $H = 1.6$ mm, $2L = 570$ mm and $G = 80$ kg

The notation is the same as in Figure 10, except that the superscripts 1, 2 and 3 refer to internal nitrogen gas pressures of $p = 63$ bar, $p = 95$ bar and $p = 125$ bar, respectively.

The $p = 0$ case has no superscript.

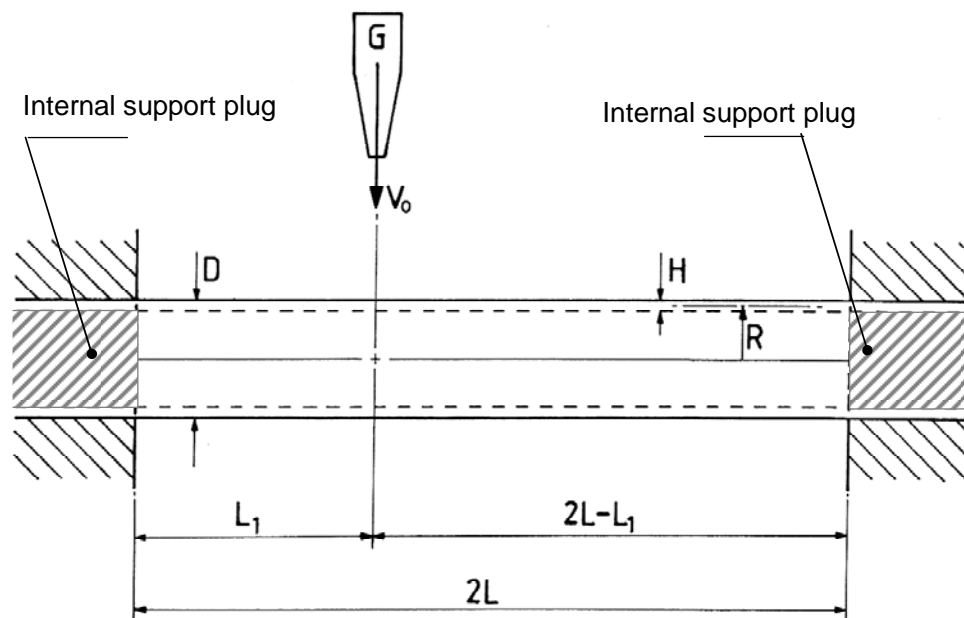
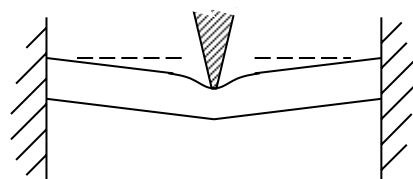


FIGURE 1

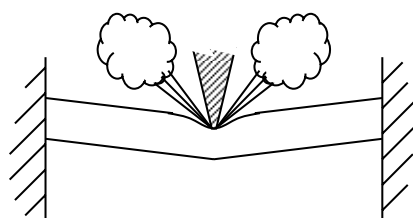


FIGURE 2

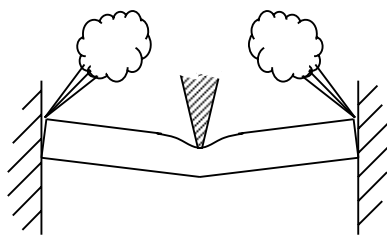
ACCEPTED



(a)



(b)



(c)

FIGURE 3

ACCEPTED MANUSCRIPT

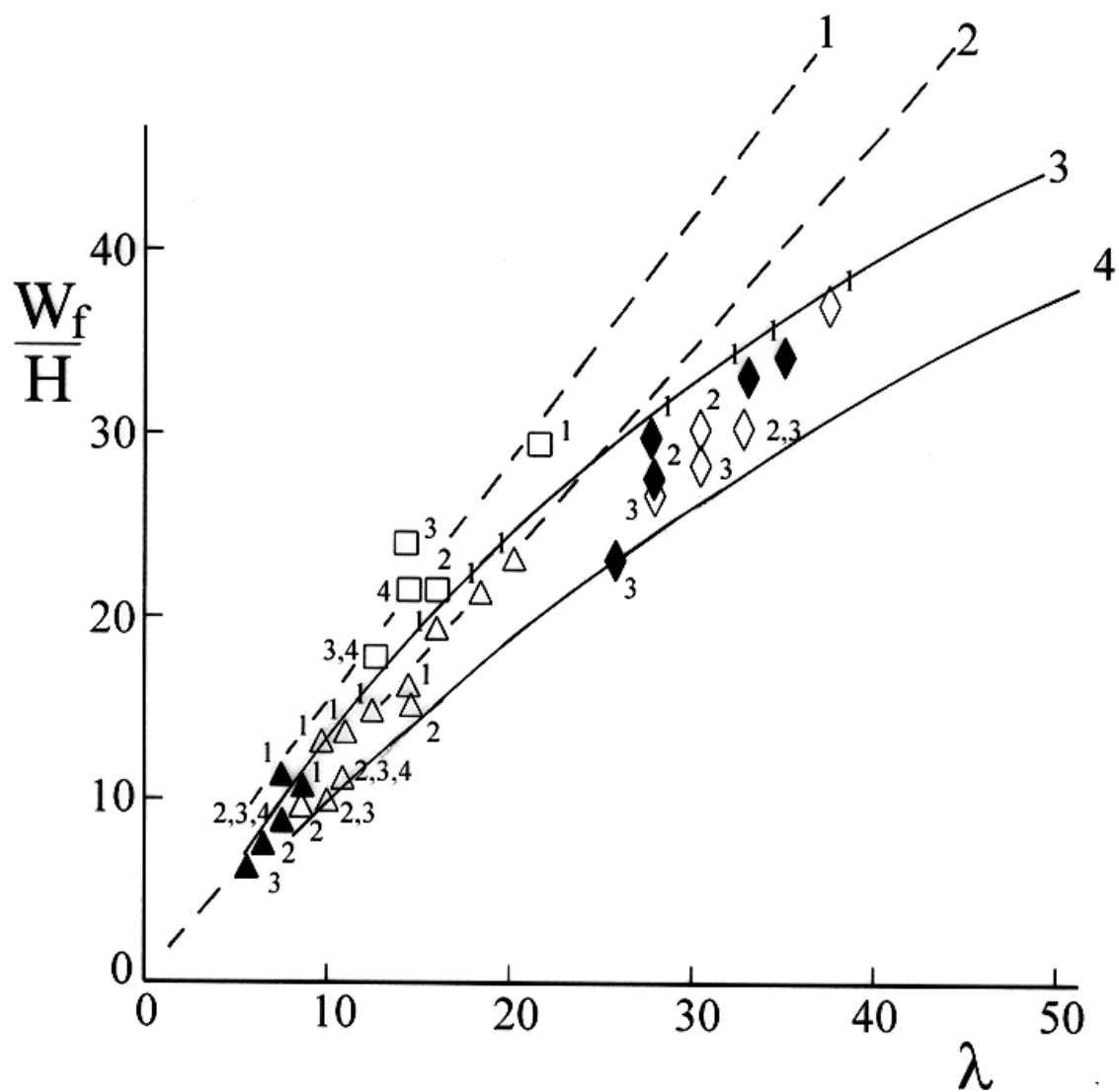


FIGURE 4

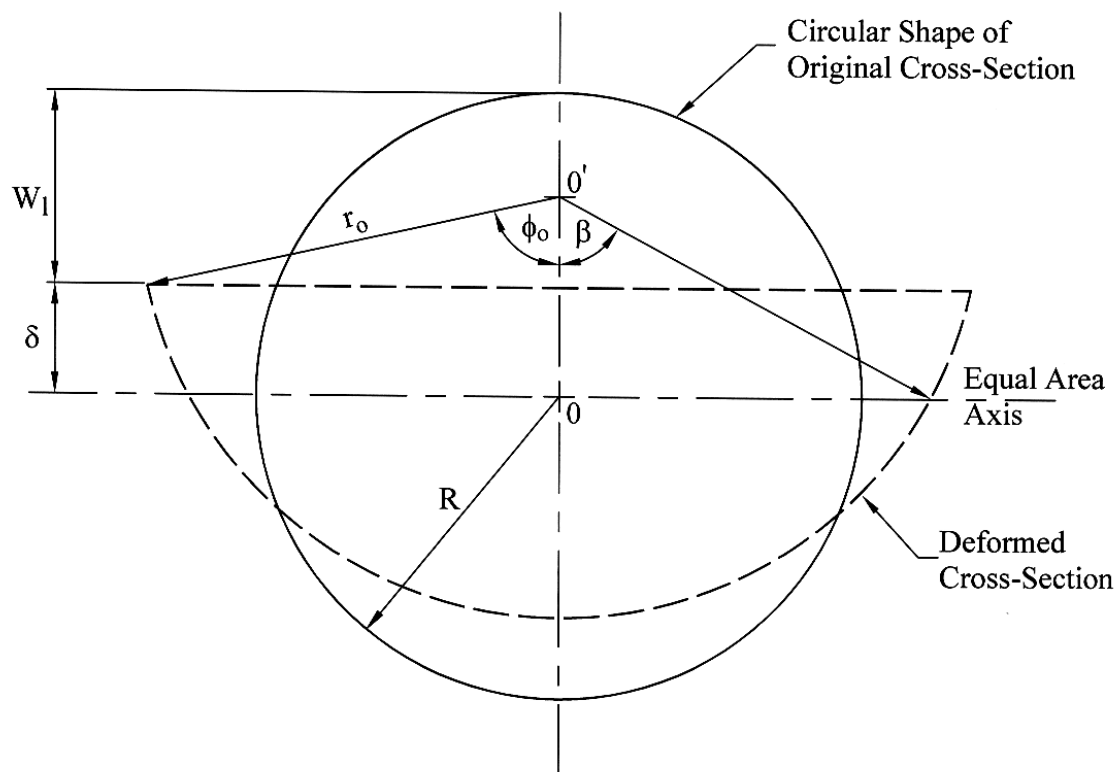


FIGURE 5

ACCEPTED

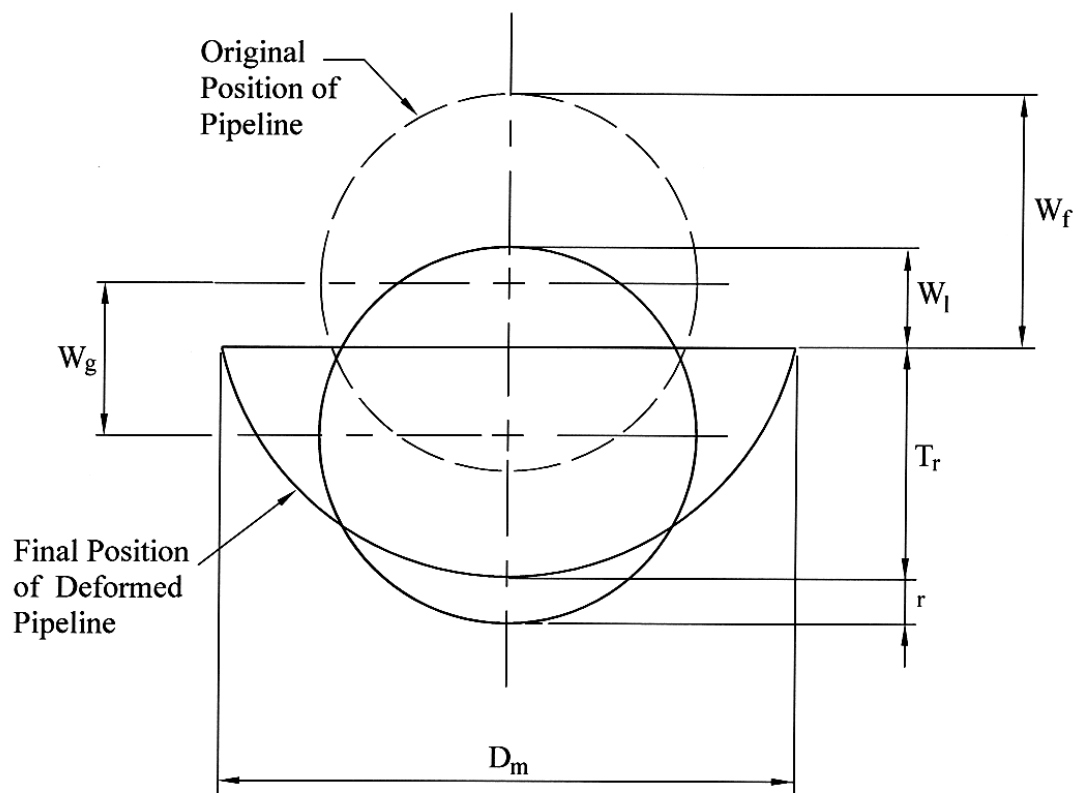


FIGURE 6

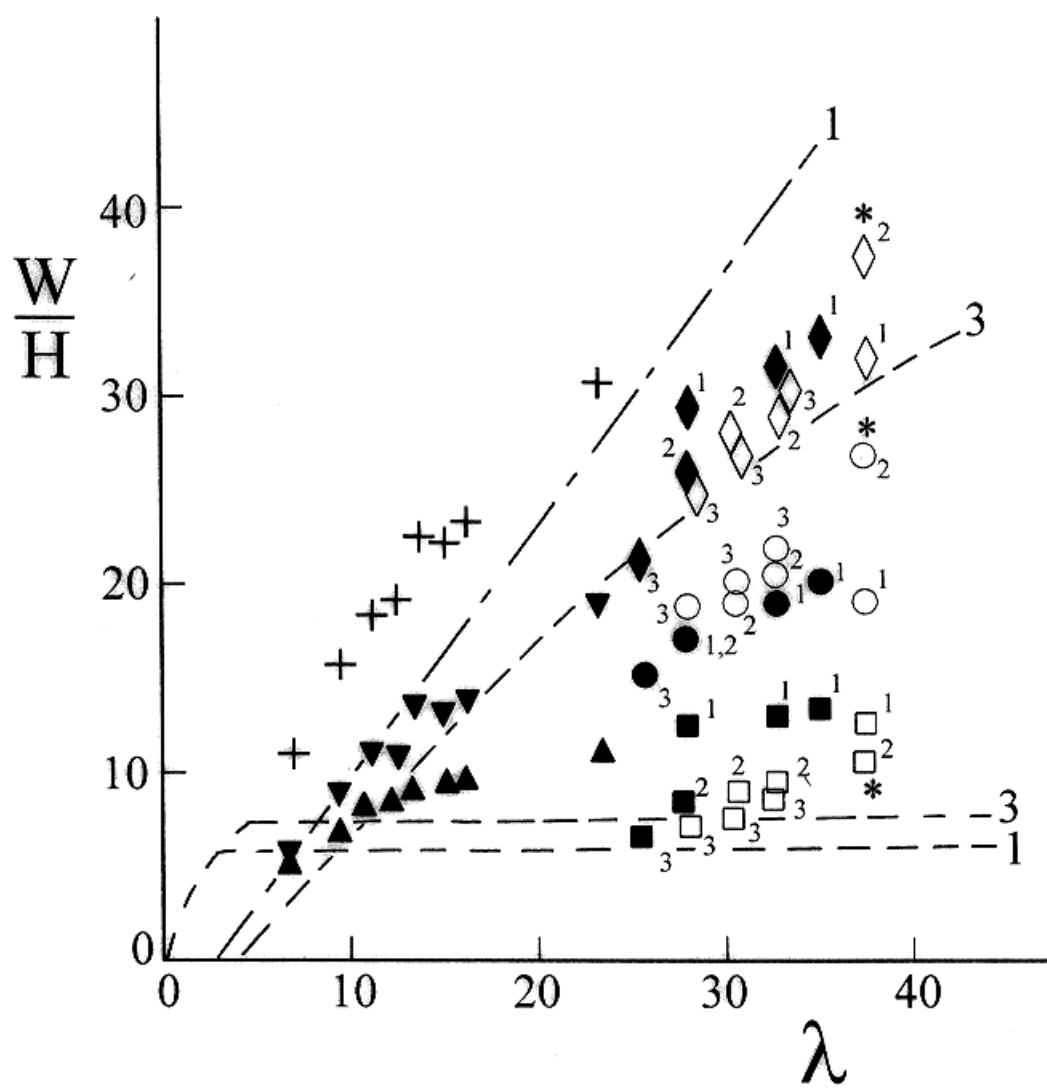


FIGURE 7

ACCE

FIGURE 8

ACCEPTED MANUSCRIPT

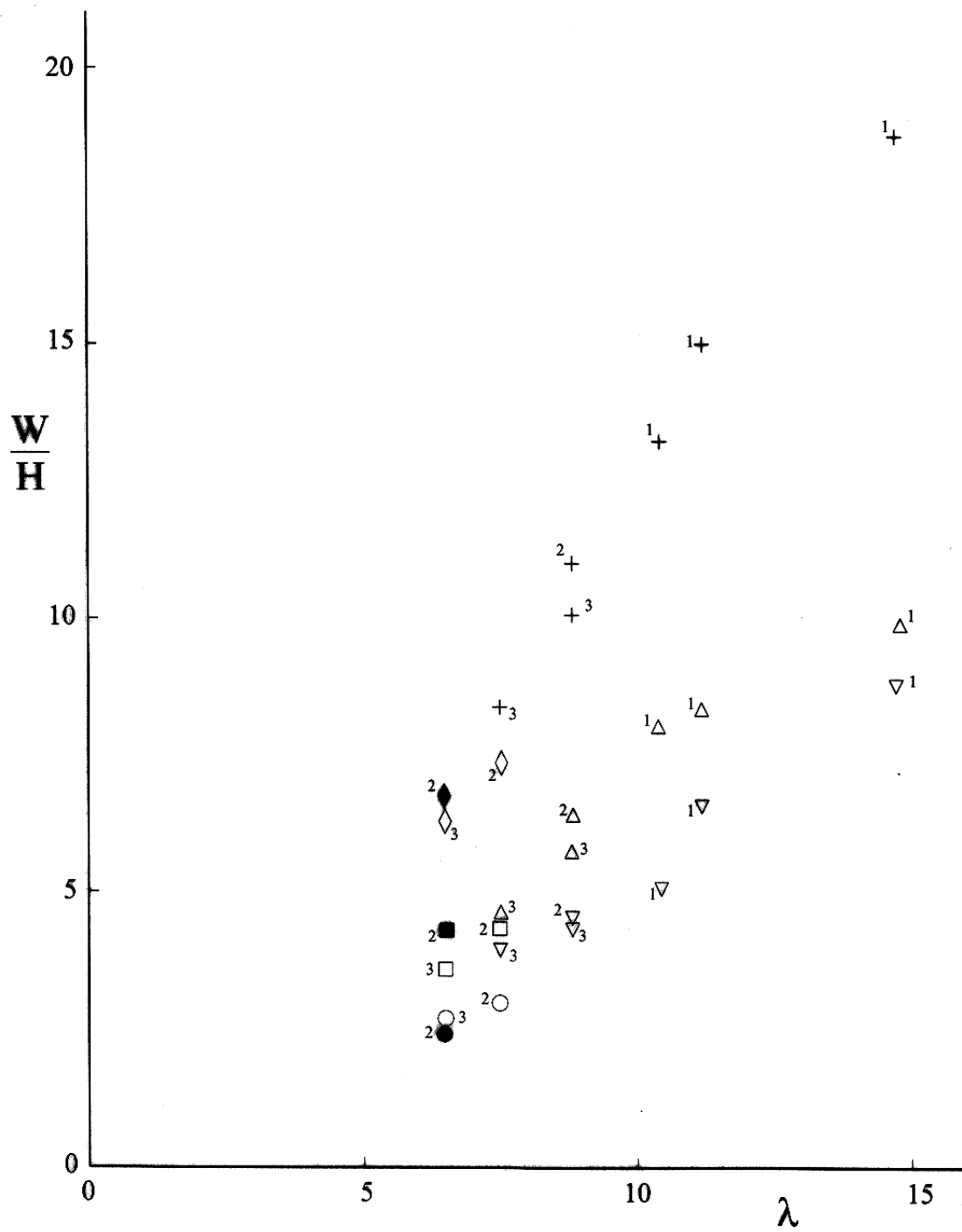


FIGURE 9

ACCEPTED MANUSCRIPT

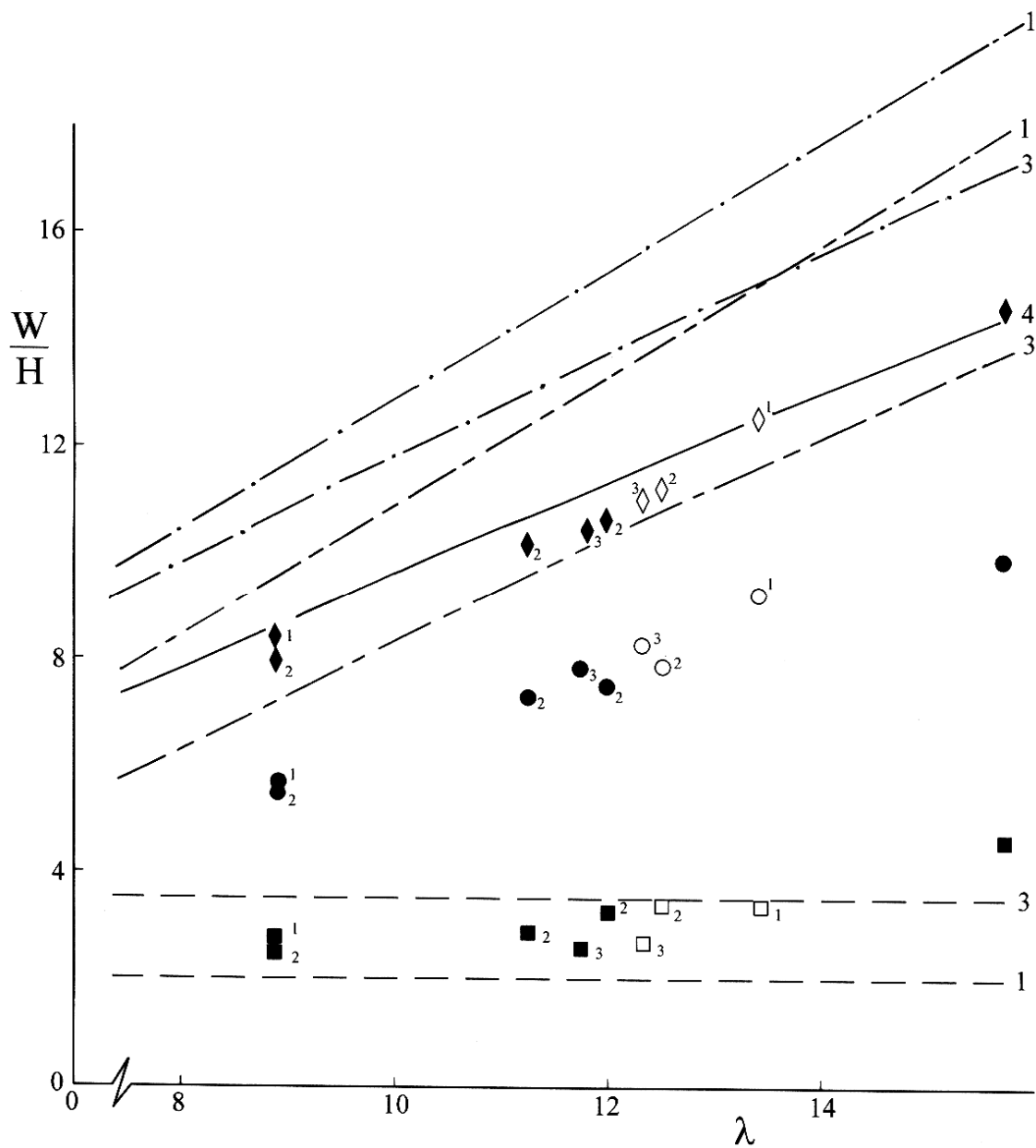


FIGURE 10

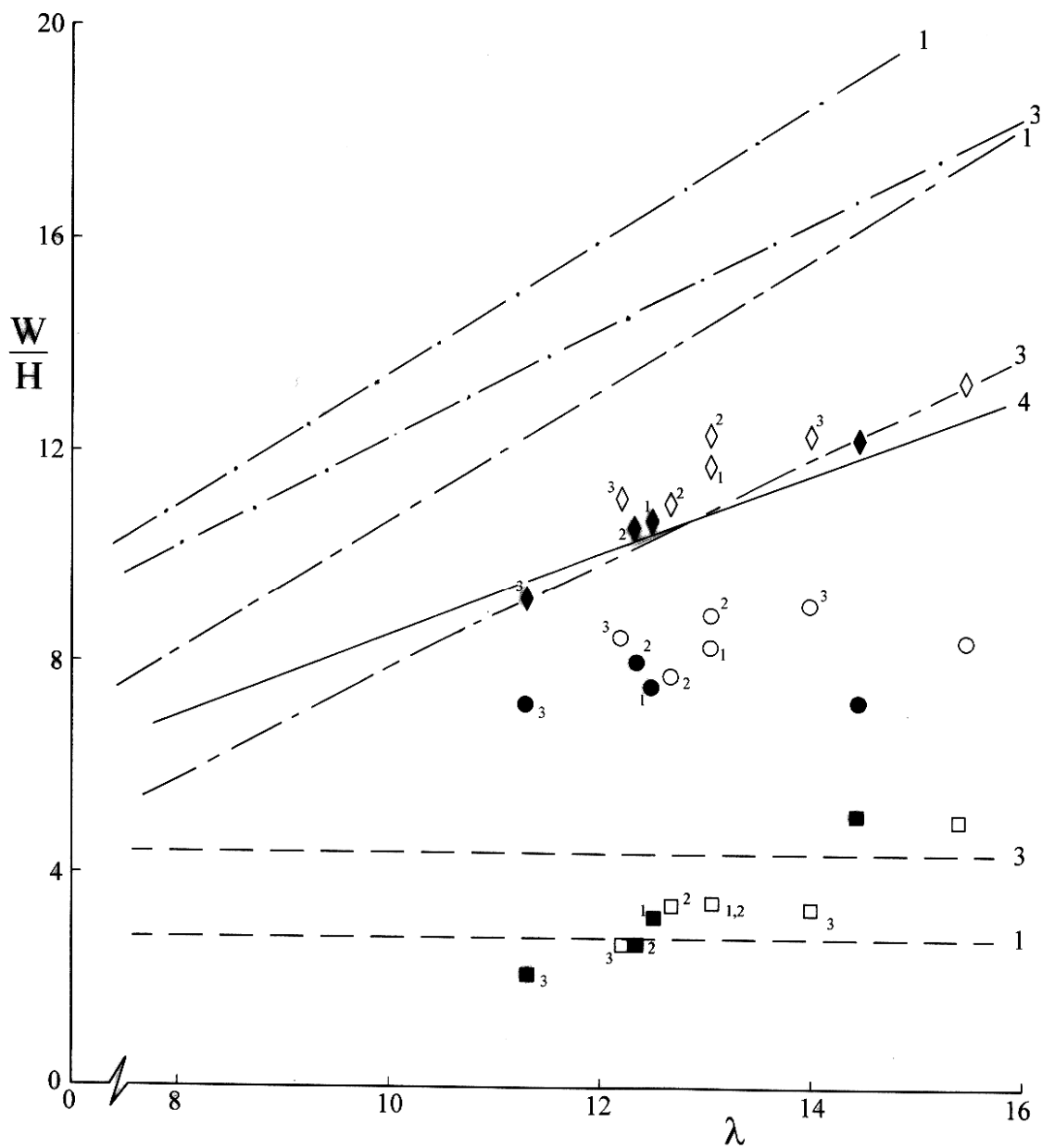


FIGURE 11

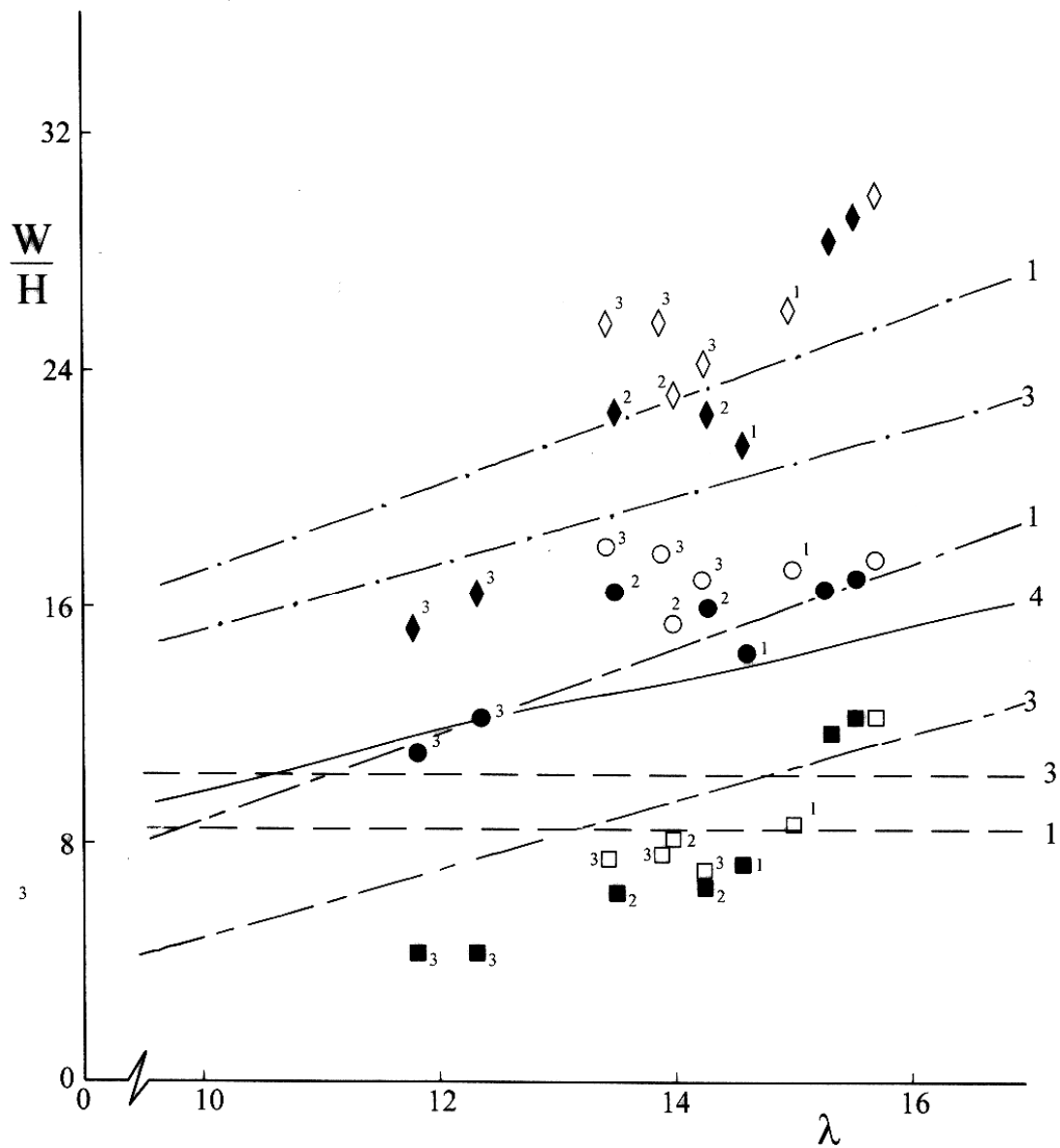


FIGURE 12